www.cafetinnova.org

Indexed in
Scopus Compendex and Geobase Elsevier,
Geo-Ref Information Services-USA, List B of Scientific Journals, Poland, Directory of Research Journals

ISSN 0974-5904, Volume 09, No. 03

International Journal of Earth Sciences and Engineering

June 2016, P.P.93-99

Simulation of Damage of Waterfront Structure of Port of Kobe during Hyogo-ken Nanbu Earthquake by Using Three-Dimensional Non-linear Parallel Finite Element Analysis

JAFRIL TANJUNG[1] AND MAKOTO KAWAMURA[2]

[1]*Civil Engineering Department, Engineering Faculty, Andalas University, Padang, 25163, INDONESIA*
[2]*Architecture and Civil Engineering Department, Toyohashi University of Technology, 1-1 Hibarigaoka, Tenpaku-cho, Toyohashi, 441-8580, JAPAN*
Email: *jafriltanjung@ft.unand.ac.id, kawamura@ace.tut.ac.jp*

Abstract: The Hyogo-ken Nanbu earthquake January 17th, 1995 caused major damage of the harbor facilities constructed in Hansin region. Most of waterfront structures, i.e. gravity caisson quay wall type, were laterally moved toward the seawater area and settled in a few meters. The site investigation after the earthquake made clear that there was reduction of the stiffness of the saturated soil layers. It is considered that the reduction of the saturated soil stiffness was caused by gradually buildup excess pore water pressure. In this paper, the analytical study using three-dimensional nonlinear parallel finite element method is discussed to get better understanding of the dynamic interaction between structures and saturated soil layers that is the relation of the large movement of the waterfront structures with the reduction of the stiffness of the saturated soil layers, which was caused by strong ground motion. The analytical results of a corner part of the Port of Kobe show that the multi-directional shear stress in the saturated soil layers increase the pore water pressure excessively, and consequently, reduces the frictional resistance at the beneath of the structures. Reducing of the frictional resistance at the beneath of the structures make the structures easily to move due to their inertia forces. As the waterfront structures move toward the seawater area, the backfill-saturated soils behind the structures then fail and the stiffness of the soil layer was reduced. As a consequence, the pore water pressure was increased. The pore water pressure responding in an isotropic manner, which was effectively simulated by the current three-dimensional analysis, affected the sequence of the waterfront movement.

Keywords: *Hyogo-ken Nanbu Earthquake, 3D nonlinear finite element analysis, parallel computation, saturated soil layers, soil structure interaction problem*

1. Introduction

Port of Kobe is located on an artificial island, Port Island, southwest side of Kobe City, Japan. The island was constructed within period 1966 and 1981 for the first stage, and the second stage was started reclaimed on 1986. Up to 1995 have been landfilled about 755 ha. The caisson gravity quay walls were constructed as waterfront structures in this port. Those structures were constructed on loose saturated decomposed granite which had been used to replace the alluvial clay layer in order to attain the required bearing capacity for the structure foundations [1].

On January 17th, 1995 the Hyogo-ken Nanbu earthquake caused great damage of these waterfront structures. They displaced about one to five meters toward the seawater area, settled approximately one to two meters and titled about four degrees. It was believed that the displaced of the waterfront structures are caused by decreasing of the stiffness soil layers beneath and behind of the waterfront structures. Soil investigation after earthquake on the Kobe Port site had proved it presumption as it was shown as low values of the Standard Penetration Test results [2, 3].

In order to simulate the damage of the waterfront structures mentioned above, however requires an accurate estimate of the complex dynamic interaction between of the waterfront structures and the saturated soil layers. One of source a complexity comes from the dynamic response of the saturated soil layers where the soil grains and the pore water interact each other. In the previous study, authors have developed three-dimensional non-linear parallel finite element computer codes, which is applicable for analyzing the dynamic interaction between structures and saturated soil layers [4, 5, 6]. In the current study, the computer codes have been extended to capture the hydrodynamic effect of the seawater wave.

2. Review Formulation of 3D Nonlinear Parallel Finite Element Method (FEM)

The parallel 3D nonlinear parallel FEM in this study was developed in the basis of the Domain Decomposition Method to separate a whole of interest domain into several non-overlapping subdomains. A traction force was introduced to enforce the continuity condition on the subdomain interfaces such that a boundary value problem then can be converted into an

interface problem [7, 8, 9]. A weighted residual method was applied to governing equations written in Eqs (1) and (2) to define the spatial discretization of the finite element. A shape function was used as the weight function [10, 11, 12, 13]. In order to achieve an efficient parallel algorithm, the balancing processor load works and inter-processor communication should be considered. The works in each processor should be balanced as possible and the inter-processor communication should be as less as possible. To satisfy it consideration, the parallel algorithm was implemented as a Single Program Multiple Data programming model. By this algorithm, the inter-processor communication was only required when solving the interface problem.

$$\sigma_{ij,i} - \rho\, \ddot{u}_i - \rho_f\, \ddot{w}_i = 0 \tag{1}$$

$$p_{,i} - \rho_f \left(\ddot{u}_i + \frac{\ddot{w}_i}{f} \right) - \frac{\rho_f\, g}{k} \dot{w}_i = 0 \tag{2}$$

In the equations above, σ_{ij} denote the components of total stress of the saturated soil, p is the pore water pressure; u_i and w_i are the components of displacement of the soil grain and the displacement of the pore water relative to u_i, respectively. The superposed dot implies time derivative; $(\,)_{,i}$ denotes the derivative with respect to coordinates x_i. For σ_{ij} and p tensile stresses are defined positive. k is the permeability and g is the gravitational acceleration. These governing equations of motion were derived by assuming the saturated soils compose of the soil grains and the pore water as is written in Eq (3).

$$\rho = (1-f)\rho_g + f\,\rho_f \tag{3}$$

Where f is the porosity, ρ is the density of the saturated soil, ρ_g is density of the soil grains and ρ_f is fluid density. The constitutive relations for the above governing equations were derived following works of Dafalias [14] as are written in Eqs (4) and (5). For the saturated soil, the constitutive relation is expressed in total stress, i.e. as a summation of the effective stress and the pore water pressure. The constitutive relation for the pore water was obtained by applying the mass conservation law to the flow of the pore water in saturated soil layer.

$$\dot{\sigma}_{ij} = D_{ijkl}\, \dot{\varepsilon}_{kl} + \alpha^2\, \delta_{ij} K_{gf} \delta_{kl}\, \dot{\varepsilon}_{kl} + \alpha\, K_{gf} \delta_{ij}\, \dot{\zeta} \tag{4}$$

$$\dot{p} = K_{gf} \left(\alpha\, \dot{\varepsilon}_{ii} + \dot{\zeta} \right) \tag{5}$$

Where

$$\frac{1}{K_{gf}} = \frac{1}{K_g} + \frac{1}{K_f} \tag{6}$$

$$a = 1 - \frac{d_{ij} D^{ep}_{ijkl} d_{kl}}{3K_g} \tag{7}$$

$$\dot{\varepsilon}_{ij} = \tfrac{1}{2}\left(u_{i,j} + u_{j,i} \right) \tag{8}$$

$$\dot{\zeta} = w_{i,i} \tag{9}$$

In which $\dot{\sigma}$ and $\dot{p}$ are the rate of the total stress and the pore water pressure, respectively. K_g, K_f and K_{gf} are the bulk module of the soil grains, the pore water and coupling of the soil grain with the pore water, respectively. α is a measure of compressibility of the soil grains representing the contact areas of the soil grains to the pore water. D^{ep}_{ijkl} represents the elasto-plastic stress-strain relation of the soil grain. d_{ij} is the component of the Kronecker's delta. $\dot{\varepsilon}_{ij}$ and $\dot{\zeta}$ are the strain rate of soil grains and the volumetric strain rate of the pore water, respectively. The elasto-plastic stress-strain relation D^{ep}_{ijkl} is expressed in Eq (10).

$$D^{ep}_{ijkl} = D^{e}_{ijkl} - u(L)\, \frac{D^{e}_{ijmn}\, P_{mn}\, Q_{pq}\, D^{e}_{pqkl}}{H + Q_{ab}\, D^{e}_{abcd}\, P_{cd}} \tag{10}$$

L is a loading index; u(L) is the heavy-step function, i.e. u(L)=1 for L $\geq$0 and u(L)=0 for L<0; D^{e}_{ijkl} is the elastic stress-strain relation; P_{ij} are the components of the plastic strain direction; Q_{ij} are the components of the normal direction to the yield surface and H is the plastic hardening modulus. In order to specify the elasto-plastic stress-strain relation in Eq (10), a simplified bounding surface plasticity model has been introduced by authors referring the previous study of Dafalias and Crouch and Wolf [14, 15]. Detail explanation about its plasticity model has been well documented by authors in references [4, 5].

The final equation of motion for the finite element analysis then can be written as in Eq (11).

$$\sum_{s=1}^{Ns} \left[\mathbf{M}^{(s)} \ddot{\mathbf{d}}^{(s)} + \mathbf{D}^{(s)} \dot{\mathbf{d}}^{(s)} + \mathbf{K}^{(s)} \dot{\mathbf{d}}^{(s)} \right] = \sum_{s=1}^{Ns} \left[\mathbf{F}^{(s)} - \mathbf{B}^{(s)^T} \boldsymbol{\lambda} \right] \tag{11}$$

With respect to the continuity condition,

$$\sum_{s=1}^{Ns} \mathbf{B}^{(s)} \mathbf{d}^{(s)} = \mathbf{0} \tag{12}$$

Where s denotes subdomain number; Ns is number of subdomains; $\mathbf{M}^{(s)}$, $\mathbf{D}^{(s)}$ and $\mathbf{K}^{(s)}$ are the mass, damping and stiffness matrices for each subdomain. The stiffness matrix **K** consists of the tangent stiffness matrix for the soil grains part, the equivalent stiffness matrix for the pore water and the stiffness of the coupling of the soil grains and the pore water. $\boldsymbol{\lambda}$ is traction forces on the interface of each subdomain. **d** is the displacement vector; superposed dot indicates time derivative. The matrix $\mathbf{B}^{(s)}$ signs the Boolean matrix, which localizes a subdomain quantity to the subdomain interface. For solving the equation of

motion written in Eq (11), the Hilber-α for constant time step Δt was applied by using the following approximation [13].

$$\mathbf{d}_n^{(s)} = \mathbf{d}_{n-1}^{(s)} + \Delta\mathbf{d}_n^{(s)} \quad (13)$$

$$\dot{\mathbf{d}}_n^{(s)} = \frac{\bar{\gamma}}{\bar{\beta}\,\Delta t}\Delta\mathbf{d}_n^{(s)} + \left(1-\frac{\bar{\gamma}}{\bar{\beta}}\right)\dot{\mathbf{d}}_{n-1}^{(s)} + \left(1-\frac{\bar{\gamma}}{2\bar{\beta}}\right)\Delta t\,\ddot{\mathbf{d}}_{n-1}^{(s)} \quad (14)$$

$$\ddot{\mathbf{d}}_n^{(s)} = \frac{1}{\bar{\beta}\,\Delta t^2}\Delta\mathbf{d}_n^{(s)} - \frac{1}{\bar{\beta}\,\Delta t}\dot{\mathbf{d}}_{n-1}^{(s)} + \left(1-\frac{1}{2\bar{\beta}}\right)\ddot{\mathbf{d}}_{n-1}^{(s)} \quad (15)$$

$$\tfrac{1}{3} \le \bar{\alpha} \le 0;\ \bar{\gamma} = \frac{1-2\bar{\alpha}}{2};\ \bar{\beta} = \frac{(1-\bar{\alpha})^2}{4} \quad (16)$$

The subscripts n and Δ in the above equations are introduced for signing a time step number and an increment, respectively. Solution of the equation of motion is obtained by substituting the Eqs (13), (14) and (15) into Eq (11). Finally, converts the time-integrated equation of motion from the boundary value problem into an interface problem. For each non-linearity iteration k, the equations may be written as follow.

$$\sum_{s=1}^{Ns}\left[\mathbf{B}^{(s)}\hat{\mathbf{K}}_n^{(s)^{-1}}\mathbf{B}^{(s)^T}\right]{}^{(k)}\Delta\boldsymbol{\lambda}_n = \sum_{s=1}^{Ns}\left[\mathbf{B}^{(s)}\hat{\mathbf{K}}_n^{(s)^{-1}}{}^{(k)}\Delta\mathbf{R}_n^{(s)}\right] \quad (17)$$

With respect to the continuity condition

$$\sum_{s=1}^{Ns}\mathbf{B}^{(s)}\,{}^{(k)}\Delta\mathbf{d}_n^{(s)} = \mathbf{0} \quad (18)$$

Where

$$\hat{\mathbf{K}}_n^{(s)} = \frac{1}{\bar{\beta}\,\Delta t^2}\mathbf{M}^{(s)} + \frac{\bar{\gamma}}{\bar{\beta}\,\Delta t}\mathbf{D}_{n-1}^{(s)} + \mathbf{K}_n^{(s)} \quad (19)$$

$${}^{(k)}\Delta\mathbf{R}_n^{(s)} = \hat{\mathbf{F}}_n^{(s)} - \sum_{j=1}^{k-1}\left(\hat{\mathbf{K}}_n^{(s)}\,{}^{(j)}\Delta\mathbf{d}_n^{(s)}\right) \quad (20)$$

$$\Delta\hat{\mathbf{F}}_n^{(s)} = \left(\mathbf{F}_n^{(s)} - \mathbf{F}_{n-1}^{(s)}\right) + \left(\frac{1}{\bar{\beta}\,\Delta t}\mathbf{M}^{(s)} + \frac{\bar{\gamma}}{\bar{\beta}}\mathbf{D}_{n-1}^{(s)}\right)\dot{\mathbf{d}}_{n-1}^{(s)} + \left(\frac{1}{2\bar{\beta}}\mathbf{M}^{(s)} + \left(\frac{\bar{\gamma}}{2\bar{\beta}}-1\right)\Delta t\,\mathbf{D}_{n-1}^{(s)}\right)\ddot{\mathbf{d}}_{n-1}^{(s)} \quad (21)$$

At first, the increment of traction forces $\Delta\boldsymbol{\lambda}$ is defined in parallel manner by using an iterative solver of the Conjugate Gradient algorithms. Further, the increment of displacement vector for each subdomain at current iteration k can be calculated by Eq (22).

$${}^{(k)}\Delta\mathbf{d}_n^{(s)} = \hat{\mathbf{K}}_n^{(s)^{-1}}\left({}^{(k)}\Delta\mathbf{R}_n^{(s)} - \mathbf{B}^{(s)^T}\,{}^{(k)}\Delta\boldsymbol{\lambda}_n\right) \quad (22)$$

The iterative process for solving the non-linearity is terminated when satisfy to a given convergence criterion. The stresses state is evaluated based on the above displacement increment. Finally, the dynamic response for each subdomain at current time step can be computed using Eqs (13), (14) and (15) in term of the displacement, the velocity and the acceleration vectors, respectively. Detail explanation of these algorithms has been well documented by author in reference [5].

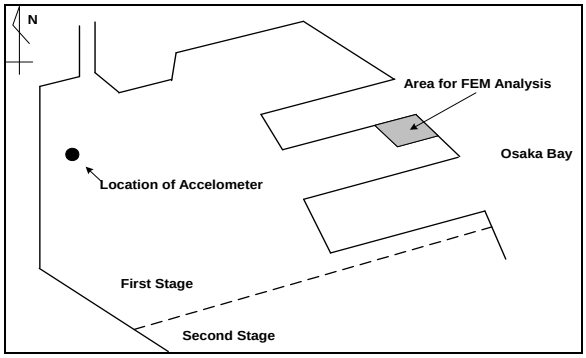

Figure 1 *Site Map of the First Stage of the Port Island*

3. Finite Element Analysis Model

For a finite element analysis model, a corner part of the first stage of the Port Island as is shown in the dark area in Figure 1 has been chosen. The dimensions of the finite element model are 276 meters long, 240 meters wide and 48 meters depth. The model was meshed into more than 12000 of 8-node brick isoparametric elements and resulting more than 50000 degrees of unknowns. The model was partitioned into 14 subdomains and was solved by using 14 individual processors in the SGI Origin/2000 machine. Partitioning of the meshed models is shown in Figure 2 and Figure 3 for the seawater and the soil layer/structures areas, respectively.

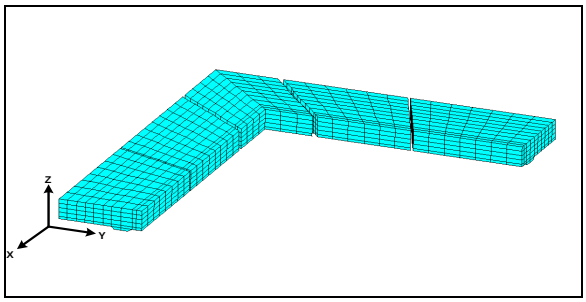

Figure 2 *Mesh Partition of Finite Element Seawater Model*

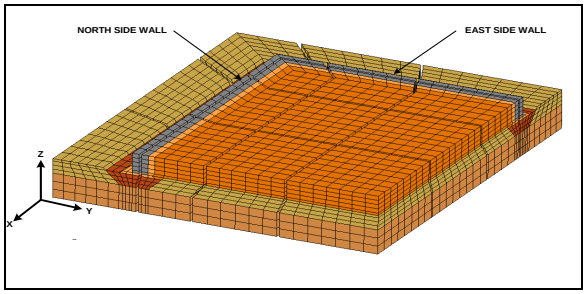

Figure 3 *Mesh Partitions of Finite Element Soil Layer and Structure Model*

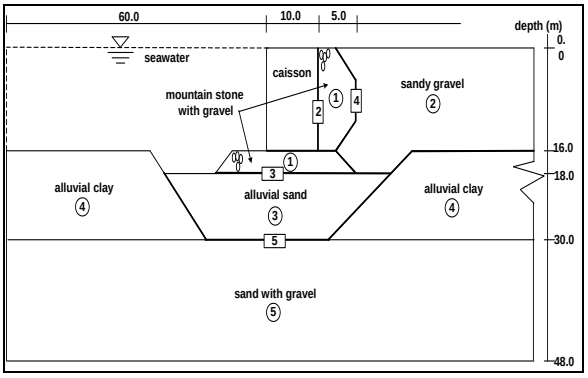

Figure 4 *Typical Cross-section of the Finite Element Analysis Model*

In the finite element analysis model, the waterfront structures, i.e. the gravity caisson quay walls, were treated as an equivalent homogenous solid material and stress-strain relation was assumed to follow the linear elastic response with small strain amplitudes. The soil layers behind and below the structures were idealized as a two-phase system coupling of the soil grains and the pore water. The stress strain relation for the soil grains was represented by the simplification of the bounding surface plasticity model. Its plasticity model has been described in detail by authors in references [4,5]. The simplified bounding surface plasticity model has 8 parameters to be determined for a particular soil type. These parameters defining the soil layer properties were determined using the standard tests results as were reported in reference [2] for the soil layers located in the Port Island. Then, these parameters were compared to the works of Wolf-Crouch [15] and Been [16]. The parameters' values for the structure and the soil layers marked in the circled number shown in the cross section of the finite element analysis model in Figure 4, are tabulated in Table 1.

Table 1: *Material Properties of the Waterfront Structure and the Soil Layers*

Property	Symbol	Unit	Caisson	Layer 1	Layer 2	Layer 3	Layer 4	Layer 5
Elastic shear modulus	G	kN/m^2	2.6×10^6					
Effective frictional angle	ϕ_{cr}	degree		33	31	32	38	35
Slope of isotropic cons. line	λ			0.035	0.06	0.02	0.25	0.13
Slope of elastic rebound line	κ			0.004	0.0021	0.0026	0.05	0.015
Parameter def. shape of ellipse	R			2.25	2.25	2.25	2.25	2.25
Elastic nucleus parameter	s_e			1.0	1.0	1.0	1.0	1.0
Hardening shape factor	hc1/hc2			0.1/0.001	0.03/0.002	0.03/0.001	0.04/0.1	0.03/0.01
	he1/he2			0.1/0.001	0.03/0.002	0.03/0.001	0.04/0.1	0.03/0.01
Initial void ratio	e_{in}			0.5	0.35	0.392	1.4	0.5
Poisson's ratio	ν		0.25	0.25	0.32	0.342	0.33	0.334
Bulk modulus of granular soil	K_g	kN/m^2		4.0×10^7	4.0×10^7	3.7×10^7	2.3×10^7	3.8×10^7
Bulk modulus of pore water	K_f	kN/m^2		2.08×10^6	2.08×10^6	2.08×10^6	2.08×10^6	2.08×10^6
Density of saturated soil	ρ	kN/m^3		27.0	26.0	23.0	27.0	26.0
Density of dried	ρ_d	kN/m^3	17.0					
Density of pore water	ρ_f	kN/m^3		10.0	10.0	10.0	10.0	10.0
Coefficient of permeability	k	m/s		1.0×10^{-2}	1.0×10^{-2}	1.2×10^{-3}	1.2×10^{-7}	7.0×10^{-5}

Table 2: *Material Properties for the Joint Surface Element*

Property	Symbol	Unit	Joint 1	Joint 2	Joint 3	Joint 4	Joint 5
Normal Stiffness	k_n	kN/m^3	1.0×10^7	1.0×10^6	1.0×10^6	1.0×10^6	1.0×10^6
Shear Stiffness	ks	kN/m^3	2.5×10^3	1.6×10^4	1.2×10^5	1.2×10^5	0.75×10^4
Friction angle	ϕ	degree	38	35	35	35	36
Hardening parameter	h		0.0001	0.01	0.01	0.01	0.01

The joint surface elements were introduced based on the two-dimensional isoparametric element to represent the interaction between the waterfront structures and the soil layers. The joint surface elements were also placed between the soil layers. Formulation of this joint surface element was derived following works of Beer [17] and Toki [18] in term of the traction force and relative displacement behavior on the surface of the element. The parameters for defining the joint surface element properties were collected from several sources such as were reported in references [17,18,19]. The parameters' values for the joint surface element marked in the boxed number shown in Figure 4, are tabulated in Table 2.

The equation of motion for the seawater wave was derived based on the total fluid energy of the fluid movement, the potential energy on the surface wave and the kinematics energy affected by the velocity of the wave as has been proposed by Wilson and Mehdi [20]. The hydrodynamic affect of the seawater was approached by uses the displacement of the seawater as the unknown. The fluid strain energy was considered according to the linear 'strain-displacement' relation and associated with the

compressibility of the fluid. The method involves the introduction of the 'constrain' of zero fluid rotation at the integration point of the fluid element. To eliminate the increment of the fluid stiffness due to high order integration, the method uses reduced integration point to produce a single element fluid 'stiffness' matrix. The material properties for the seawater elements are only bulk modulus of the water K_f and a non-dimensional multiplier constant for defining the rotational bulk modulus of the water α_r. A value of bulk modulus of the water K_f was taken as 2.08 x 106 kN/m^2 and Wilson and Mehdi [20] have recommended a value of αr as 100.

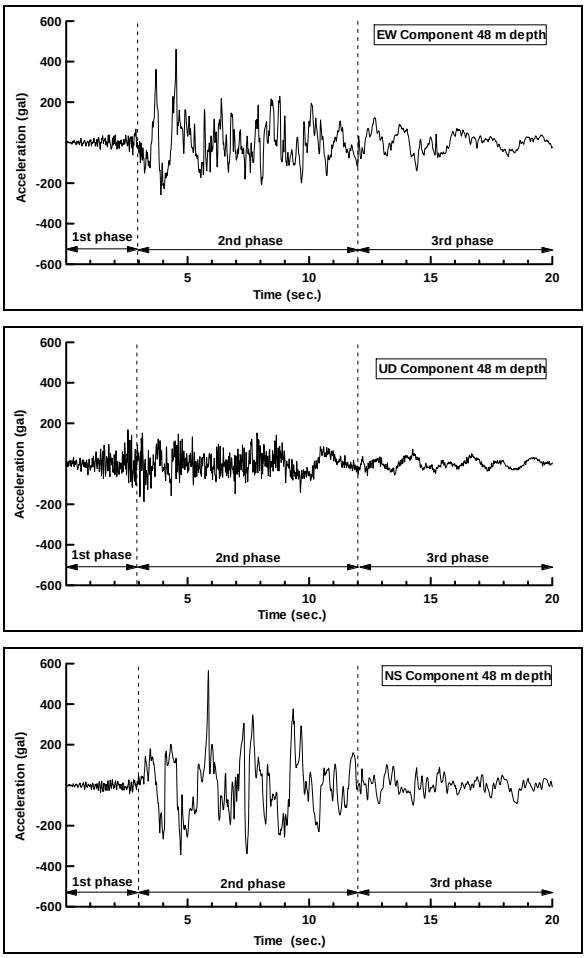

Figure 5 *Acceleration Recorded at Port Island during 1995 Hyogo-Ken Nanbu Earthquake*

Except for the upper surface of the finite element analysis model, both of soil grains and the pore water were not allowed to move outward on the boundaries of the model. The pore water pressures on the upper surface of the finite element analysis model were kept equal to zero during the analysis. The surface wave of the seawater was enforced by their potential energy such that the hydrodynamic pressures remain constant even for large vertical movement.

The model was subjected to three components of ground motion recorded by the accelerometer at the depth of 48 meters below the surface of the Port Island. A location of the accelerometer is marked as a filled circle in Figure 1. The accelerations of these ground motions are plotted in Figure 5. The analysis was conducted for 15 seconds excitation with constant time step $\Delta t = 0.005$ second and Hilber-α parameter -0.25.

4. Analytical Results and Discussion

As was previously noted that the Hyogo-ken Nanbu earthquake, 1995 caused major damage of the harbor facilities constructed in Hansin region. Most of gravity caisson quay wall type of the waterfront structures were laterally moved toward the seawater area and settled in a few meters. These waterfront blocks separated one to each other's. Several of them were overturning respect to their original position. This phenomenon has been made clear by the analytical results of the current parallel 3D finite element analysis as is shown in Figure 6. A good agreement has been obtained when the analytical results are compared to the observed results as are plotted in Figure 7.

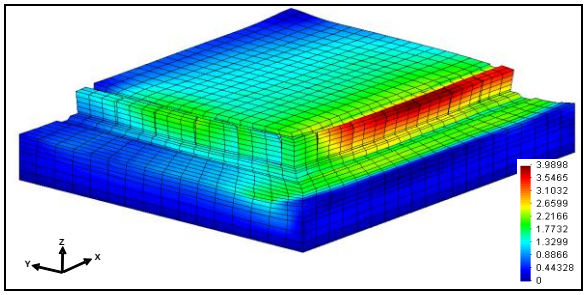

Figure 6 *Deformation of the Analytical Model*

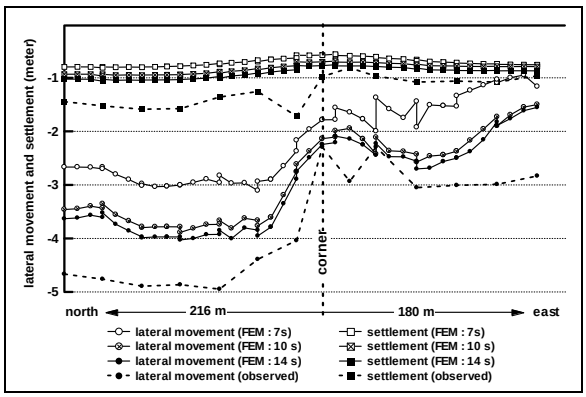

Figure 7 *Analytical and Observed Comparison of Lateral Movement and Settlement of the Waterfront Structures*

To understand the reasons of the large movement of these structures, at first consider the increasing of the pore water pressures as is shown in time history of the pore water pressure at beneath of waterfront structures in Figure 8. Increasing of these pore water pressures were induced by the multi-direction shear stress in the saturated soil layers as the consequences of the multi-direction of the applied ground motion into the finite

element model. As the results, the frictional resistance at the beneath of the waterfront structures will be significantly reduced, and therefore, make the waterfront structures easily to move due to their inertia forces.

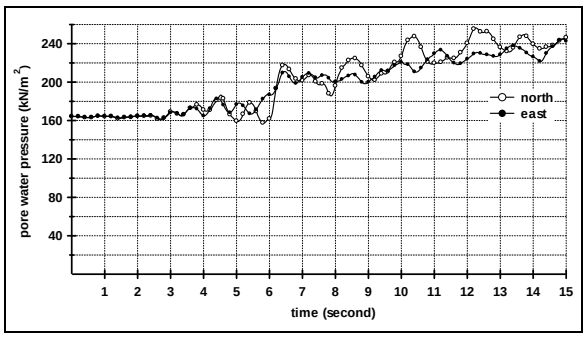

Figure 8 *Time History of the Pore Water Pressures Acting at Beneath of the Waterfront Structure*

When the waterfront structures start to move, the pore water pressures will excessively increase in the saturated soil layers at the behind of the waterfront structure and at the same time will reduces the effective stress of the soil grains. Reduction of the effective stress the saturated soil layers are clearly shown in the effective stress path at behind of the waterfront structures in Figure 9 and Figure 10 for the north and the east structures, respectively. These figures shows that the mean effective stress significantly reduces and the deviatoric stress going to critical state line. These reductions will directly reduce the stiffness and the bearing capacity of the saturated soil layers.

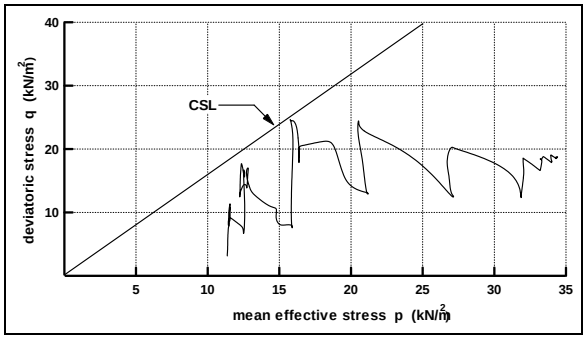

Figure 9 *Effective Stress Path at Behind of the North Waterfront Structure*

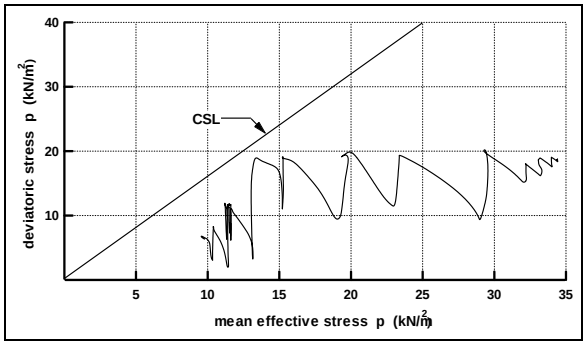

Figure 10 *Effective Stress Path at Behind of the East Waterfront Structure*

5. Conclusions

The current three-dimensional parallel finite element algorithm has been successfully simulated the damaged of the waterfront structures in the Port of Kobe during Hyogo-Ken Nanbu earthquake, 1995. The damaged of the waterfront structures were initially caused by increasing the pore water pressure which was induced by multi-directional shear stress in the saturated soil layer beneath the waterfront structures. Increasing the pore water pressure causes reduction of the frictional resistance at the beneath of the structures and makes the structures easy move due to their inertia force. Simultaneous lateral movement and highly build up excess pore water pressure will reduced the bearing capacity of the soil layers. In this study, a good agreement was also obtained when the analytical results of the large movement of the waterfront structures are compared to the field observation after earthquake.

References

[1] Yang, J., Sato, T., and Li, X.S., Nonlinear Site Effects on Strong Ground Motion at a Reclaimed Island, *J. Can. Geotech.*, Vol. 37, pp. 26-39, 2000.

[2] Ministry of Transport, *Damage to port and port-related facilities by the 1995 Hyogo Ken Nanbu Earthquake*, The Port and Harbour Research Institute, Japan, 1997.

[3] Madabhushi, S.P.G., *Strong Motion at Port Island During the Kobe Earthquake*, Research CUED/D-SOILS/TR285, Cambridge University, 1995.

[4] Kawamura, M., and Tanjung, J., 3D Nonlinear Parallel FEM Analysis for Seismic Earth Pressures of Saturated Soil Layer, *Journal of Structural Engineering/Earthquake Engineering, JSCE*, Vol 19 No.2, pp 199s-129s, 2002.

[5] Tanjung, J., 3D Nonlinear Parallel FEM for Analyzing Dynamic Response of a Large-Scale Saturated Soil Layers-Civil Structures Interaction Problem (Part I: Formulation and its Numerical Solution), *Jurnal Teknik Sipil ITB*, Vol. 17 No. 2, pp. 81-90, 2010.

[6] Tanjung, J., 3D Nonlinear Parallel FEM for Analyzing Dynamic Response of a Large-Scale Saturated Soil Layers-Civil Structures Interaction Problem (Part II: Verification and Performance), *Jurnal Teknik Sipil ITB*, Vol. 17 No. 3, pp. 153-161, 2010.

[7] Tallec, P.L. and Vidrascu, M., Solving Large Scale Structural Problems on Parallel Computers using Domain Decomposition Techniques, *Parallel Solution Methods in Computational Mechanics* (Ed. Papadrakakis, M.), John Wiley & Sons, Chichester, 1997.

[8] Papadrakakis, M., Domain Decomposition Techniques for Computational Structural Mechanic, *Parallel Solution Methods in Computational Mechanics* (Ed. Papadrakakis, M.), John Wiley & Sons, Chichester, 1997.
[9] Farhat, C. and Roux, F.X., A Method of Finite Element Tearing and Interconnecting and Its Parallel Solution Algorithm, *Int. Journal for Num. Methods Engg.*, Vol. 32, pp, 1205-1227, 1991.
[10] Ghaboussi, A.M. et al., Seismic Analysis of Earth Dam Reservoir System, *J. Soil Mech. And Found. Div., ASCE.*, Vol.99, No. SM10, pp. 849-862, 1973.
[11] Zienkiewicz, O.C and T. Shiomi, Dynamic Behavior of Saturated Porous Material, The Generalized Biot Formulation and Its Numerical Solution, *Int. J. Num. Anal. Meth. Geomech.*, Vol. 8, pp. 71-96, 1984.
[12] Zienkiewicz, O.C and R. L. Taylor, *The Finite Element Method*, McGraw-Hill, London,1991.
[13] Hughes, T.J.R., *The Finite Element Method Linear Static and Dynamic Finite Element Analysis*, Prentice Hall, New Jersey, 1996.
[14] Dafalias, Y. F., Bounding Surface Plasticity I, Mathematical Foundation and Hypoplasticity, *Journal of Eng. Mech. Geomech*, Vol. 112, No. 12, pp, 966-987, 1986.
[15] Crouch, R. S. and J.P. Wolf, Unified 3D Critical State Bounding Surface Plasticity Model for Soils incorporating Continues Plasticity Loading Under Cyclic Path, Constitutive Relations, *Int. Journal. Num. Anal. Met., Geomech.*, Vol. 18, pp, 735-758, 1994.
[16] Been, K., Jefferies, M.G., and Hachey, J., , The Critical State of Sands, *Geotechnique*, Vol. 41, No. 3, pp. 365-381, 1991.
[17] Beer, G. , An Isoparametric Joint/Interface Element for Finite Element Analysis, *Int. Journal Num. Meth. Engg.*, Vol. 21, pp.585-600, 1985.
[18] Toki, K., Sato, T., and Miura, E., Separation and Sliding Between Soil and Structure During Strong Ground Motion, *Journal of Earthquake Engineering Structural Dynamics.*, Vol. 9, pp. 263-277, 1981.
[19] Hazarika, H. and H. Matsuzawa, Coupled Shear Band Method and Its Application to Seismic Earth Pressure Problem, *Soils and Foundation, JSSMFE*, Vol. 37, No. 3, pp. 65-77, 1997.
[20] Wilson, E.L. and Mehdi, K., Finite Elements for the Dynamic Analysis of Fluid-Solid Systems, *Int. J. for Num. Meth. Engg.*, Vol. 19, pp.1657-1668, 1983.